

# Impedance and resistivity of low-Pt cathode in a PEM fuel cell

Andrei Kulikovsky<sup>a)</sup>

*Forschungszentrum Jülich GmbH*

*Institute of Energy and Climate Research,*

*IEK-13: Theory and Computation of Energy Materials*

*D-52425 Jülich, Germany*<sup>b)</sup>

(Dated: 20 March 2021)

Analysis of impedance model for the low-Pt cathode catalyst layer (CCL) in a PEM fuel cell is reported. The CCL is modeled as a cylindrical pore with the Nafion film separating the open pore volume from the Pt/C surface. In the limit of fast oxygen transport through the open pore, analytical expressions for the CCL impedance, Nafion film impedance and for the ohmic CCL resistivity  $R_{ccl}$  ( $\text{Ohm cm}^2$ ) are derived. The characteristic frequency of film impedance is independent of film oxygen transport parameters and it is only 1.73 times less than the frequency of faradaic process in the CCL, which impedes separation of these processes by impedance spectroscopy.  $R_{ccl}$  exhibits rapid growth in the vicinity of limiting current density in the Nafion film, manifesting “overlinear” oxygen transport loss reported in experiments. For typical low-Pt cell parameters, this growth occurs at the cell current around  $1 \text{ A cm}^{-2}$ . The model leads to a simple relation for the Nafion film transport resistance  $\mathcal{R}_N$  ( $\text{s cm}^{-1}$ ); this relation is compared to semi-empirical and model relations available in literature.

Keywords: PEM fuel cell, low-Pt loaded cathode, impedance, modeling

## I. INTRODUCTION

Lowering of Pt loading in PEM fuel cells is of tremendous importance for success of PEMFC-based power sources. Currently, Pt loading on the cell cathode is  $0.4 \text{ mg}_{\text{Pt}} \text{ cm}^{-2}$ , which translates to about 100 g of precious metal in a 100-kW automotive PEMFC stack.

Attempts to lower Pt loading on the cathode side have revealed unexpected overlinear loss of the cell performance in the region of high cell currents<sup>1,2</sup>. The effect is illustrated in Figure 1 showing polarization curves of the cells with the cathode Pt loading differing by a factor of three. As can be seen, below  $1 \text{ A cm}^{-2}$ , the polarization curve of the low-Pt cell ( $0.12 \text{ mg}_{\text{Pt}} \text{ cm}^{-2}$ ) is parallel to the curve of high-Pt cell ( $0.35 \text{ mg}_{\text{Pt}} \text{ cm}^{-2}$ ). In this region of currents, lowering of the cell potential of a low-Pt cell is “linear”, due to reduced cathode electrochemical surface area. However, above  $1 \text{ A cm}^{-2}$ , the low-Pt cell potential exhibits faster (“overlinear”) decay, which increases with the cell current (shaded area).

This effect has been attributed to oxygen transport in the Nafion film covering Pt/C agglomerates<sup>2–7</sup>. In standard, high-Pt cells the role of this process is marginal, while in low-Pt cells at high currents, oxygen transport through the Nafion

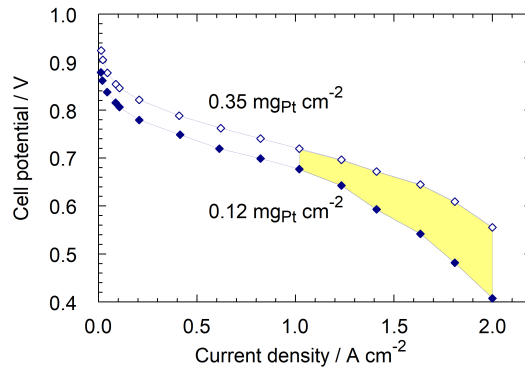


FIG. 1. Experimental polarization curves of two cells with the indicated Pt loading on the cathode side. The data have been digitized from Figure 1 in the paper of Ono et al.<sup>1</sup>.

<sup>a)</sup> ECS Active member; Electronic mail: A.Kulikovsky@fz-juelich.de

<sup>b)</sup> Also at: Lomonosov Moscow State University, Research Computing Center, 119991 Moscow, Russia

film gives quite substantial contribution to the voltage loss. In simple terms, lower amount of the oxygen reduction reaction (ORR) sites in the electrode means higher proton current density and hence higher oxygen flux per each site, making the Nafion film barrier a significant hurdle for oxygen transport to the site. An alternative, or rather complementary explanation of overlinear transport loss is based on the idea that the low-Pt CCL is prone to flooding<sup>8</sup>.

A relation between the Nafion film resistivity  $\mathcal{R}_N$  ( $\text{s cm}^{-1}$ ) and the film transport parameters still is not fully understood. Semi-empirical equations for  $\mathcal{R}_N$  have been suggested in<sup>6,9</sup> (see discussion below). Chen et al.<sup>10</sup> developed a Lattice-Boltzmann pore-scale model, taking into account oxygen diffusion in ionomer and faradaic process. Oxygen transport resistance of the electrode was calculated using the numerical simulation results. Ono et al.<sup>1</sup> developed a numerical transmission line model for oxygen transport in the electrode, which includes Tafel kinetics for the ORR. Due to numerical nature of their model, no analytical result for  $\mathcal{R}_N$  has been reported. Numerical model of Moore et al.<sup>11</sup> does not suggest analytical approximations for the film resistivity. Mashio et al.<sup>12</sup> developed an analytical model for oxygen transport into a single porous carbon particle covered by Nafion film. They derived an expression for the film transport resistance discussed below. Hao et al.<sup>13</sup> suggested analytical formula for the film resistance taking into account interfacial resistance and oxygen transport through water. However, their formula contains parameters which need to be determined from the numerical CFD model of the fuel cell.

Recently, Schuler et al.<sup>14</sup> reported measurements of transport resistivity of a low-Pt cathode catalyst layer by means of hydrogen limiting current method. The experimental data have been processed using the continuum model for hydrogen mass transport through the electrode at limiting current density. The results show hyperbolic-like growth of the CCL transport resistivity with the decrease in Pt loading of the electrode. This dependence qualitatively agrees with the measurements of Ono et al.<sup>1</sup>, Owejan et al.<sup>3</sup> and Nonoyama et al.<sup>9</sup>. A detailed literature review of the problem is given in<sup>14</sup>.

A tool very sensitive to transport processes in fuel cell is electrochemical impedance spectroscopy (EIS). In<sup>15</sup> impedance spectra of a low-Pt cell have been measured and a numerical model for cell impedance, which explicitly takes into account oxygen transport through the Nafion film has been fitted to experimental spectra. Fitting returns the Nafion film thickness  $l_N$  and the film oxygen diffusivity  $D_N$ ; the ratio of  $l_N/D_N$  has been taken as an estimate of the film oxygen transport resistivity  $\mathcal{R}_N$ .

Below, the analysis of model equations<sup>15</sup> is performed. Analytical solution for the CCL impedance is derived for the case of fast oxygen transport through the void pore and of nearly uniform static overpotential through the CCL depth. This solution leads to simple expressions for the Nafion film impedance and for the CCL ohmic resistivity  $R_{ccl}$  ( $\text{Ohm cm}^2$ ). The characteristic frequency of film impedance is independent of film oxygen transport parameters and it is close to the frequency of faradaic process in the cell. The resistivity  $R_{ccl}$  exhibits the effect of limiting current due to oxygen transport through the film. The expression for  $R_{ccl}$  leads to a simple formula for the Nafion film transport resistance  $\mathcal{R}_N$  ( $\text{s cm}^{-1}$ ). The dependence of  $\mathcal{R}_N$  on Pt loading in the electrode fits well recent experimental data. The formula for  $\mathcal{R}_N$  is compared to semi-empirical and model equations suggested in literature.

## II. MODEL

### A. Transient equations

The cathode catalyst layer (CCL) is modeled by a single cylindrical pore penetrating through the CCL depth. The pore is “inserted” into a metallic tube representing Pt/C particles surrounding a real pore. The pore volume is separated from the metal surface by a thin coaxial Nafion film (Figure 2). The model is suitable for description of Pt/C electrodes with Vulcan type of carbon support and Pt nanoparticles residing on the outer surface of carbon spheres. The equations of this subsection have been discussed in detail in Ref.<sup>15</sup>. For completeness and due to some corrections, the equations are briefly described below.

Let the pore and metal radii be  $R_p$  and  $R_m$ , respectively, and let the membrane be located at  $x = 0$  and the GDL be located at  $x = l_t$  (Figure 2). Oxygen transport along the pore axis  $x$  is described by the transient diffusion equation

$$\frac{\partial c}{\partial t} - D_p \frac{\partial^2 c}{\partial x^2} = \frac{2}{R_p} N_{N,p}, \quad \frac{\partial c}{\partial x} \Big|_{x=0} = 0, \quad c(l_t) = c_1, \quad (1)$$

where  $c$  is the oxygen concentration,  $c_1$  is this concentration at the CCL/GDL interface,  $D_p$  is the oxygen diffusion coefficient in the pore volume,  $l_t$  is the CCL thickness (the pore length), and  $N_{N,p}$  is the oxygen flux in the Nafion film at the pore/film interface, directed along the radius  $r$

$$N_{N,p} = D_N \frac{\partial c_N}{\partial r} \Big|_{r=R_p+}. \quad (2)$$

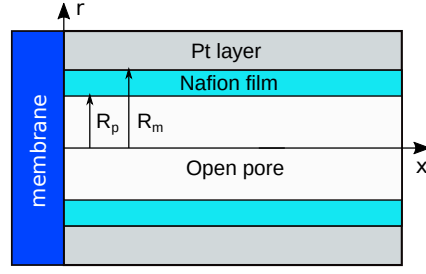


FIG. 2. Schematic of the single-pore model for the cathode catalyst layer.

Here,  $D_N$  is the effective oxygen diffusivity in the film. The factor  $2/R_p$  in Eq.(1) and the factor  $2R_m/R_p^2$  in Eq.(3) below provide the balance of oxygen fluxes in the pore volume and correct transition of the model to the standard macro-homogeneous model of the CCL performance in the limit of zero Nafion film thickness<sup>16</sup>. Note that in the first version of the model<sup>15</sup> the oxygen flux at the film/metal interface was used in Eq.(1). Calculations show that the flux (2) in Eq.(1) makes the model more sensitive to Nafion film parameters.

Oxygen transport along the radial direction in the Nafion film is described by the diffusion equation

$$\frac{\partial c_N}{\partial t} - \frac{D_N}{r} \frac{\partial}{\partial r} \left( r \frac{\partial c_N}{\partial r} \right) = 0, \quad c_N(R_p) = K_H c(x), \quad -D_N \frac{\partial c_N}{\partial r} \Big|_{r=R_m} = \left( \frac{R_p^2}{2R_m} \right) \frac{i_*}{4F} \left( \frac{c_{N,m}}{c_h^{in}} \right) \exp \left( \frac{\eta}{b} \right) \quad (3)$$

where  $c_N$  is the oxygen concentration in the film,  $K_H$  is the dimensionless Henry's constant for oxygen dissolution in Nafion film. The second boundary condition for Eq.(3) means that the oxygen flux at the Nafion film/metal interface equals the Tafel rate of the oxygen consumption in the ORR. Here,  $c_{N,m}$  is the oxygen concentration at the film/metal interface,  $c_h^{in}$  is the reference concentration,  $i_*$  is the volumetric exchange current density of the ORR,  $\eta$  is the positive by convention ORR overpotential, and  $b$  is the ORR Tafel slope.

The system is completed by the proton current conservation equation

$$C_{dl} \frac{\partial \eta}{\partial t} + \frac{\partial j}{\partial x} = -i_* \left( \frac{c_{N,m}}{c_h^{in}} \right) \exp \left( \frac{\eta}{b} \right), \quad (4)$$

where  $j$  is the local proton current density in the Nafion film and  $C_{dl}$  is the double layer capacitance. Using Ohm's law

$$j = -\sigma_N \frac{\partial \eta}{\partial x} \quad (5)$$

we eliminate  $j$  from Eq.(4), which gives

$$C_{dl} \frac{\partial \eta}{\partial t} - \sigma_N \frac{\partial^2 \eta}{\partial x^2} = -i_* \left( \frac{c_{N,m}}{c_h^{in}} \right) \exp \left( \frac{\eta}{b} \right) \quad (6)$$

where  $\sigma_N$  is the Nafion film proton conductivity. The CCL electronic conductivity is assumed to be large and the respective potential loss is ignored.

The system of equations (1), (3) and (6) forms a basis for construction of the impedance model. To simplify further calculations, it is convenient to introduce the dimensionless variables

$$\tilde{t} = \frac{t}{t_*}, \quad \tilde{x} = \frac{x}{l_t}, \quad \tilde{r} = \frac{r}{l_t}, \quad \tilde{c} = \frac{c}{c_h^{in}}, \quad \tilde{j} = \frac{j}{j_*}, \quad \tilde{\eta} = \frac{\eta}{b},$$

$$\tilde{D}_N = \frac{4FD_N c_h^{in}}{\sigma_N b}, \quad \tilde{D}_p = \frac{4FD_p c_h^{in}}{\sigma_N b}, \quad \tilde{\omega} = \omega t_*, \quad \tilde{Z} = \frac{Z \sigma_N}{l_t} \quad (7)$$

where

$$t_* = \frac{C_{dl} b}{i_*}, \quad j_* = \frac{\sigma_N b}{l_t} \quad (8)$$

are the characteristic time of double layer charging and the characteristic current density for proton transport, respectively. With these variables, Eqs.(1), (3) and (6) take the form

$$\mu^2 \frac{\partial \tilde{c}}{\partial \tilde{t}} - \varepsilon_*^2 \tilde{D}_p \frac{\partial^2 \tilde{c}}{\partial \tilde{x}^2} = \gamma_p \varepsilon_*^2 \tilde{N}_{N,p}, \quad \frac{\partial \tilde{c}}{\partial \tilde{x}} \Big|_{\tilde{x}=0} = 0, \quad \tilde{c}(1) = \tilde{c}_1, \quad (9)$$

$$\mu^2 \frac{\partial \tilde{c}_N}{\partial \tilde{t}} - \varepsilon_*^2 \frac{\tilde{D}_N}{\tilde{r}} \frac{\partial}{\partial \tilde{r}} \left( \tilde{r} \frac{\partial \tilde{c}_N}{\partial \tilde{r}} \right) = 0, \quad \tilde{c}_N(\tilde{R}_p) = K_H \tilde{c}(\tilde{x}), \quad -\gamma_m \varepsilon_*^2 \tilde{D}_N \frac{\partial \tilde{c}_N}{\partial \tilde{r}} \Big|_{\tilde{r}=\tilde{R}_m} = \tilde{c}_{N,m} \exp \tilde{\eta} \quad (10)$$

$$\frac{\partial \tilde{\eta}}{\partial \tilde{t}} - \varepsilon_*^2 \frac{\partial^2 \tilde{\eta}}{\partial \tilde{x}^2} = -\tilde{c}_{N,m} \exp \tilde{\eta}, \quad \tilde{\eta}(0) = \tilde{\eta}_0, \quad \frac{\partial \tilde{\eta}}{\partial \tilde{x}} \Big|_{\tilde{x}=1} = 0 \quad (11)$$

where the dimensionless parameters are given by

$$\mu = \sqrt{\frac{4F\tilde{c}_h^{in}}{C_{dl}b}}, \quad \varepsilon_* = \sqrt{\frac{\sigma_N b}{i_* l_t^2}}, \quad \gamma_p = \frac{2}{\tilde{R}_p}, \quad \gamma_m = \frac{2\tilde{R}_m}{\tilde{R}_p^2} \quad (12)$$

## B. Equations for the perturbation amplitudes

Applying in Eqs.(9), (10) and (11) perturbations of the form

$$\begin{aligned} \tilde{c} &= \tilde{c}^0(\tilde{x}) + \tilde{c}^1(\tilde{x}, \tilde{\omega}) \exp(i\tilde{\omega}\tilde{t}), \\ \tilde{c}_N &= \tilde{c}_N^0(\tilde{r}) + \tilde{c}_N^1(\tilde{r}, \tilde{\omega}) \exp(i\tilde{\omega}\tilde{t}), \\ \tilde{\eta} &= \tilde{\eta}^0(\tilde{x}) + \tilde{\eta}^1(\tilde{x}, \tilde{\omega}) \exp(i\tilde{\omega}\tilde{t}) \end{aligned} \quad (13)$$

and taking into account smallness of the perturbation amplitudes  $\tilde{c}^1$ ,  $\tilde{c}_N^1$  and  $\tilde{\eta}^1$ , we get a system of linear equations for these amplitudes

$$\varepsilon_*^2 \tilde{D}_p \frac{\partial^2 \tilde{c}^1}{\partial \tilde{x}^2} = -\gamma_p \varepsilon_*^2 \tilde{N}_{N,p}^1 + i\tilde{\omega} \mu^2 \tilde{c}^1, \quad \frac{\partial \tilde{c}^1}{\partial \tilde{x}} \Big|_{\tilde{x}=0} = 0, \quad \tilde{c}^1(1) = 0, \quad (14)$$

$$\varepsilon_*^2 \frac{\tilde{D}_N}{\tilde{r}} \frac{\partial}{\partial \tilde{r}} \left( \tilde{r} \frac{\partial \tilde{c}_N^1}{\partial \tilde{r}} \right) = i\tilde{\omega} \mu^2 \tilde{c}_N^1, \quad \tilde{c}_N^1(\tilde{R}_p) = K_H \tilde{c}^1(\tilde{x}), \quad -\gamma_m \varepsilon_*^2 \tilde{D}_N \frac{\partial \tilde{c}_N^1}{\partial \tilde{r}} \Big|_{\tilde{r}=\tilde{R}_m} = \exp(\tilde{\eta}^0) (\tilde{c}_{N,m}^1 + \tilde{c}_{N,m}^0 \tilde{\eta}^1) \quad (15)$$

$$\varepsilon_*^2 \frac{\partial^2 \tilde{\eta}^1}{\partial \tilde{x}^2} = \exp(\tilde{\eta}^0) (\tilde{c}_{N,m}^1 + \tilde{c}_{N,m}^0 \tilde{\eta}^1) + i\tilde{\omega} \tilde{\eta}^1, \quad \tilde{\eta}^1(0) = \tilde{\eta}_0^1, \quad \frac{\partial \tilde{\eta}^1}{\partial \tilde{x}} \Big|_{\tilde{x}=1} = 0 \quad (16)$$

where  $\tilde{\eta}_0^1$  is the applied potential perturbation. The superscripts 0 and 1 mark the static variables and the perturbations, respectively. In Eq.(14), the perturbed flux  $\tilde{N}_{N,p}^1$  at the pore/film interface is given by

$$\tilde{N}_{N,p}^1 = \tilde{D}_N \frac{\partial \tilde{c}_N^1}{\partial \tilde{r}} \Big|_{\tilde{r}=\tilde{R}_p+} \quad (17)$$

Note the right boundary condition for Eq.(14), meaning that the oxygen concentration at the CCL/GDL interface is not perturbed. This condition isolates the CCL problem from oxygen transport in the GDL and channel. Generally, oxygen transport in the GDL can be incorporated by using Robin-type right boundary condition for Eq.(14) instead of  $\tilde{c}^1(1) = 0$ , (see Eq.(38) in<sup>15</sup>). This, however, makes analytical treatment of the CCL problem much more difficult.

Eq.(15) decouples from the system and it can be directly solved. The solution is rather cumbersome and it is not displayed

here; important is that  $\tilde{c}_{N,m}^1$  and  $\tilde{N}_{N,p}^1$  can be expressed as a linear combination of  $\tilde{c}^1$  and  $\tilde{\eta}^1$ :

$$\tilde{c}_{N,m}^1 = \alpha_c \tilde{c}^1 + \beta_c \tilde{\eta}^1 \quad (18)$$

$$\tilde{N}_{N,p}^1 = \alpha_N \tilde{c}^1 + \beta_N \tilde{\eta}^1 \quad (19)$$

with the coefficients  $\alpha_c$ ,  $\beta_c$ ,  $\alpha_N$ ,  $\beta_N$  containing Bessel functions and static shapes of the oxygen concentration and overpotential<sup>15,17</sup>. The problem, thus, reduces to the system of linear equations, Eqs.(14), (16) for  $\tilde{c}^1$  and  $\tilde{\eta}^1$ :

$$\varepsilon_*^2 \tilde{D}_p \frac{\partial^2 \tilde{c}^1}{\partial \tilde{x}^2} = -(\gamma_p \varepsilon_*^2 \alpha_N + i\tilde{\omega} \mu^2) \tilde{c}^1 - \gamma_p \varepsilon_*^2 \beta_N \tilde{\eta}^1, \quad (20)$$

$$\varepsilon_*^2 \frac{\partial^2 \tilde{\eta}^1}{\partial \tilde{x}^2} = e^{\tilde{\eta}_0} \alpha_c \tilde{c}^1 + (e^{\tilde{\eta}_0} (\beta_c + \tilde{c}_{N,m}^0) + i\tilde{\omega}) \tilde{\eta}^1 \quad (21)$$

In general, the coefficients on the right side of Eqs.(20), (21) are functions of coordinate  $\tilde{x}$ . Nonetheless, in the limit of *nearly* fast proton transport in Nafion film and oxygen transport in the void pore, the static shapes of  $\tilde{c}^0$  and  $\tilde{\eta}^0$  can be assumed independent of  $\tilde{x}$ , retaining at the same time the coordinate dependence of the perturbations  $\tilde{c}^1(\tilde{x}, \tilde{\omega})$  and  $\tilde{\eta}^1(\tilde{x}, \tilde{\omega})$  (Ref.<sup>18</sup>). These assumptions are justified if the cell current is small

$$j_0 \ll \min \left\{ j_* = \frac{\sigma_N b}{l_t}, \quad j_{ox} = \frac{4FD_p c_1}{l_t} \right\} \quad (22)$$

Physically, Eq.(22) means that the working current density must be much less than the characteristic current densities for proton  $j_*$  and oxygen  $j_{ox}$  transport in the CCL. In this case, the system (20), (21) can be solved analytically. However, the solution is hopelessly cumbersome; math assistant Maple<sup>®</sup> returns several pages of output leaving no chances for reasonable simplification of the result.

### III. RESULTS AND DISCUSSION

#### A. Catalyst layer impedance

Useful and compact results can be obtained if we further assume ideally fast oxygen transport in the void pore and set  $\tilde{c}^1 = 0$ . The system of Eqs.(20), (21) then reduces to the single equation for  $\tilde{\eta}^1$ :

$$\varepsilon_*^2 \frac{\partial^2 \tilde{\eta}^1}{\partial \tilde{x}^2} = (e^{\tilde{\eta}_0} (\beta_c + \tilde{c}_{N,m}^0) + i\tilde{\omega}) \tilde{\eta}^1, \quad \tilde{\eta}^1(0) = \tilde{\eta}_0^1, \quad \left. \frac{\partial \tilde{\eta}^1}{\partial \tilde{x}} \right|_{\tilde{x}=1} = 0 \quad (23)$$

where

$$\beta_c = \frac{A_\eta E \tilde{c}_{N,m}^0}{B}, \quad (24)$$

$$A_\eta = J_0(q\tilde{R}_p)K_0(-iq\tilde{R}_m) - J_0(q\tilde{R}_m)K_0(-iq\tilde{R}_p) \quad (25)$$

$$B = \left( J_0(q\tilde{R}_m)K_0(-iq\tilde{R}_p) - J_0(q\tilde{R}_p)K_0(-iq\tilde{R}_m) \right) E - \left( iJ_0(q\tilde{R}_p)K_1(-iq\tilde{R}_m) + J_1(q\tilde{R}_m)K_0(-iq\tilde{R}_p) \right) q \quad (26)$$

and

$$q = \sqrt{-\frac{i\tilde{\omega}\mu^2}{\varepsilon_*^2 \tilde{D}_N}}, \quad E = \frac{e^{\tilde{\eta}_0}}{\gamma_m \varepsilon_*^2 \tilde{D}_N}. \quad (27)$$

Here,  $J_0$ ,  $J_1$  are the Bessel functions of the first kind,  $K_0$ ,  $K_1$  are the modified Bessel functions of the second kind.

For  $\tilde{\eta}^0$  and  $\tilde{c}_{N,m}^0$  independent of  $\tilde{x}$ , parameters in Eq.(23) are constant and this equation can be solved. Calculating the

impedance according to

$$\tilde{Z}_{ccl} = - \frac{\tilde{\eta}^1}{\partial \tilde{\eta}^1 / \partial \tilde{x}} \Big|_{\tilde{x}=0} \quad (28)$$

we get

$$\tilde{Z}_{ccl} = \frac{1}{\sqrt{\psi} \tanh \sqrt{\psi}} \quad (29)$$

where

$$\psi = \frac{1}{\varepsilon_*^2} \left( i\tilde{\omega} + e^{\tilde{\eta}_0} \tilde{c}_{N,m}^0 \left( 1 + \frac{A_\eta E}{B} \right) \right) \quad (30)$$

Using the Tafel law<sup>16</sup>

$$\tilde{c}_{N,m}^0 e^{\tilde{\eta}_0} = \varepsilon_*^2 \tilde{j}_0, \quad (31)$$

Eq.(30) simplifies to

$$\psi = \frac{i\tilde{\omega}}{\varepsilon_*^2} + \tilde{j}_0 \left( 1 + \frac{A_\eta E}{B} \right) \quad (32)$$

For  $e^{\tilde{\eta}_0}$  in Eq.(27), analysis of static equations<sup>16</sup> gives

$$e^{\tilde{\eta}_0} = \frac{\varepsilon_*^2 \tilde{j}_0}{K_H \tilde{c}_1 - a \varepsilon_*^2 \tilde{j}_0} \quad (33)$$

where

$$a = \frac{\tilde{R}_p^2}{2\varepsilon_*^2 \tilde{D}_N} \ln \left( \frac{\tilde{R}_m}{\tilde{R}_p} \right). \quad (34)$$

Finally, Eq.(32), with  $A_\eta$  and  $B$  given by Eqs.(25) and (26), respectively, fully determine the CCL impedance, Eq.(29), for a given cell current density  $\tilde{j}_0$ .

The impedance  $\tilde{Z}_{ctp}$  due to charge-transfer and proton transport in the CCL can be obtained if we “remove” the Nafion film by setting  $K_H = 1$  and  $\tilde{R}_p = \tilde{R}_m$  in Eq.(29). This gives

$$\tilde{Z}_{ctp} = \frac{1}{\sqrt{\tilde{j}_0 + i\tilde{\omega}/\varepsilon_*^2} \tanh \sqrt{\tilde{j}_0 + i\tilde{\omega}/\varepsilon_*^2}}, \quad (35)$$

which recovers the result<sup>19</sup>. Comparing Eq.(32) with the expression under the square root in Eq.(35) we see, that the effect of Nafion film is described by the term  $\tilde{j}_0 A_\eta E/B$  in Eq.(32). This term is proportional to  $\tilde{j}_0$  and it vanishes as the film thickness tends to zero.

## B. Nafion film impedance

An exact, but cumbersome expression for the pure Nafion film impedance  $\tilde{Z}_N$  can be obtained if we subtract the charge-transfer plus proton transport impedance, Eq.(35), from the total CCL impedance, Eq.(29):

$$\tilde{Z}_N = \tilde{Z}_{ccl} - \tilde{Z}_{ctp} \quad (36)$$

A much simpler and suitable for analysis approximate expression for  $\tilde{Z}_N$  arises if we note that the parameter  $\varepsilon_*^2 \tilde{D}_N$  is large; e.g., for parameters in Table I,  $\varepsilon_*^2 \tilde{D}_N \simeq 3 \cdot 10^4$ . This parameter appears in denominator of the argument  $q$  of the Bessel functions, Eq.(27). Thus, we can make an attempt to formally expand  $\tilde{Z}_{ccl}$  over  $\tilde{D}_N \rightarrow \infty$  in a hope that this expansion

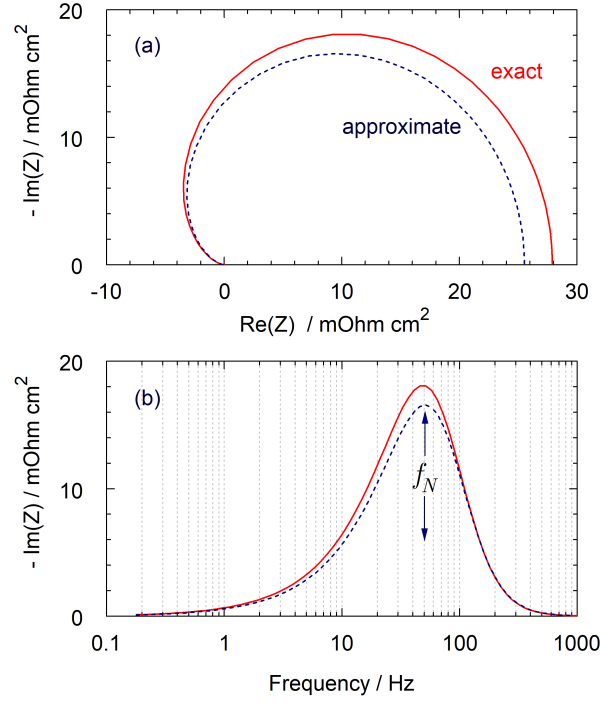


FIG. 3. (a) Exact, Eq.(36), and approximate, Eq.(38) Nyquist spectra of the Nafion film impedance. (b) The frequency dependence of imaginary part of impedances in (a). Parameters for the calculation are listed in Table I.

would work at least for sufficiently low frequencies. Keeping two leading terms of expansion, we get

$$\tilde{Z}_{ccl}^{\tilde{D}_N \rightarrow \infty} \simeq \tilde{Z}_{ctp} + \tilde{Z}_N^\infty \quad (37)$$

where  $\tilde{Z}_{ctp}$  is given by Eq.(35), and the approximate Nafion film impedance is

$$\tilde{Z}_N^\infty = \frac{\tilde{R}_p^2 \ln(\tilde{R}_m / \tilde{R}_p)}{4\tilde{c}_1 K_H \tilde{D}_N} \left( \frac{\tilde{j}_0^2}{\tilde{j}_0 + i\tilde{\omega} / \varepsilon_*^2} \right) \left( \tilde{Z}_{ctp} + \frac{2}{\cosh\left(2\sqrt{\tilde{j}_0 + i\tilde{\omega} / \varepsilon_*^2}\right) - 1} \right) \quad (38)$$

Fortunately, Eq.(38) approximates the exact  $\tilde{Z}_N$  reasonably well in the whole frequency range (Figure 3). For lower current densities the agreement of curves in Figure 3 is better. The reason is that at high frequencies, the impedance  $\tilde{Z}_{ccl}$  is determined by proton transport, which is independent of film oxygen transport parameters. This explains success of asymptotic expansion leading to Eq.(38). The spectra in Figure 3a closely resemble the Nyquist spectrum of GDL impedance (see Figure 2 in Ref.<sup>20</sup>), which suggests analogy between the oxygen transport in the GDL and Nafion film.

Of particular interest is the characteristic frequency  $f_N$  corresponding to the peak value of imaginary part of impedance (Figure 3b). Numerical calculations show that to a good accuracy  $f_N$  is approximated by

$$f_N \simeq \frac{j_0}{2\sqrt{3}\pi b C_{dl} t} \quad (39)$$

Surprisingly, Eq.(39) does not depend on the Nafion film parameters. Indeed, the pore and film parameters  $\tilde{R}_p$ ,  $\tilde{R}_m$  and  $\tilde{D}_N$  appear in Eq.(38) as a factor at the frequency-dependent terms, i.e., these parameters simply scale the absolute value of impedance  $\tilde{Z}_N^\infty$ , not affecting its frequency dependence.

The characteristic frequency of faradaic processes in PEM fuel cell is  $f_{ct} \simeq j_0 / (2\pi b C_{dl} t)$  (Ref.<sup>21</sup>). Comparing this to Eq.(39) we see that  $f_N$  is only  $\sqrt{3} \simeq 1.73$  times less, than  $f_{ct}$ . This impedes separation of the charge-transfer and film-transport processes by EIS at low currents.

Figure 4 shows the dependence of characteristic frequency  $f_N$  on the film oxygen diffusivity  $D_N$  obtained numerically as

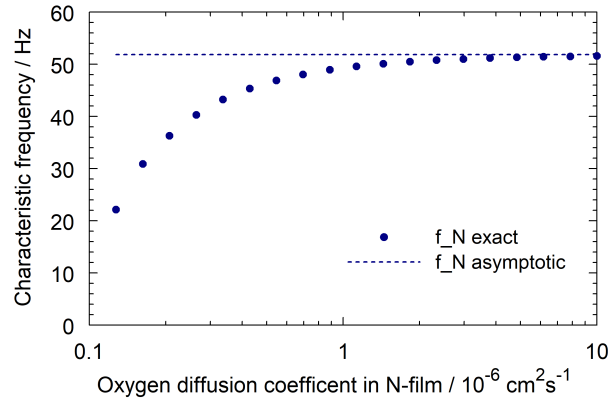


FIG. 4. Characteristic frequency  $f_N$  of oxygen transport in Nafion film as a function of oxygen diffusion coefficient  $D_N$  in the film. Points represent numerical solution of equation  $\partial \text{Im}(\tilde{Z}_N)/\partial \tilde{\omega} = 0$  with  $\tilde{Z}_N$  given by Eq.(36), dashed line – solution of the same equation with  $\tilde{Z}_N$  from Eq.(38).

a solution to equation  $\partial \text{Im}(\tilde{Z}_N)/\partial \tilde{\omega} = 0$  with  $\tilde{Z}_N$  given by Eqs.(36) and (38). For  $D_N > 10^{-6} \text{ cm}^2 \text{ s}^{-1}$ , the variation of exact numerical  $f_N$  is small, and it tends to asymptotic value of this parameter given by Eq.(38). At  $D_N$  lower than  $3 \cdot 10^{-7} \text{ cm}^2 \text{ s}^{-1}$  the asymptotic expansion (37) does not work, and exact  $f_N$  strongly deviates from the asymptotic value (Figure 4). Figure 4 and Eq.(39) suggest that at sufficiently high  $D_N$ , the frequency of oxygen transport in the film is controlled by the rate of ORR at the film/Pt interface. Note that  $D_N = 10^{-6} \text{ cm}^2 \text{ s}^{-1}$  in Table I corresponds to low currents; for higher currents this parameter grows up to  $6 \cdot 10^{-6} \text{ cm}^2 \text{ s}^{-1}$  due to increasing liquid water content in the electrode (Ref.<sup>15</sup>).

Eq.(39) is obtained for low current density, assuming fast oxygen transport in a void pore. Under these conditions,  $f_N$  appears to be insensitive to the film parameters. This property of  $\tilde{Z}_N^\infty$  makes it different from the GDL impedance with the characteristic frequency dependent on GDL thickness and oxygen diffusivity<sup>20</sup>.

It is worth noting that the present analysis ignores oxygen transport in the void pore. The characteristic frequency of pore-transport  $f_{ox}$  can be estimated using the Warburg finite-length formula  $f_{ox} \simeq 2.54 D_p / (2\pi l_t^2)$ . With  $D_p \simeq 10^{-4} \text{ cm}^2 \text{ s}^{-1}$ , we get  $f_{ox} \simeq 450 \text{ Hz}$ , which by an order of magnitude exceeds  $f_N$  in Figure 3b.

Generally, the CCL transport resistivity in low-Pt cells can be measured using the distribution of relaxation times (DRT) technique. Typical DRT spectrum contains a number of well-separated along the frequency scale peaks, which correspond to different kinetic and transport processes. In<sup>22</sup> it was assumed that the system “pore+film” forms a unified pathway for oxygen transport represented by a single DRT peak located between 500 and 1000 Hz.

The analysis of this section suggests that at low cell currents and high oxygen diffusivity in the void pore this assumption is not justified. At low currents and large  $D_P$ ,  $f_N \simeq f_{ct}/\sqrt{3}$ , hence the transport in Nafion film should form a separate DRT peak located in close proximity to the faradaic peak, on the left side of it. In this case, the rightmost peak in the DRT spectra discussed in<sup>22</sup> represents oxygen transport in the void pores only. Calculation of the DRT for Eq.(29) shows that reliable separation of Nafion film peak from the faradaic peak is hard to achieve. A fast “nnls”-version of the DRT code (Appendix) returns a single asymmetric “film + faradaic” peak at 76.8 Hz (Figure 5). The problem with Nafion film peak separation seems to be due to the domain of negative real part of the film impedance (Figure 3a). This domain cannot be expanded over the sum of  $RC$ -circuit impedances, which is prerequisite for successful calculation of DRT. The second, high-frequency peak at 12.1 kHz in Figure 5 represents proton transport in the system.

Generally, thin ionomer film is an impedance element located between two other elements with quite different characteristic frequencies: void pore and faradaic reactions. In the absence of void pore impedance, the frequency of film impedance is close to the frequency of faradaic process. Numerical calculations show that in case of large transport losses in void pore the frequency of film impedance is close to the frequency of pore impedance<sup>15</sup>. It seems that the frequency of film impedance is determined by the slowest process among the oxygen transport in void pore and faradaic reactions. This conjecture requires further experimental and modeling studies. Last but not least, the frequency position of Nafion film peak at high currents is unclear. Precise impedance measurements in combination with modeling are necessary to locate this peak in experimental DRT spectra.



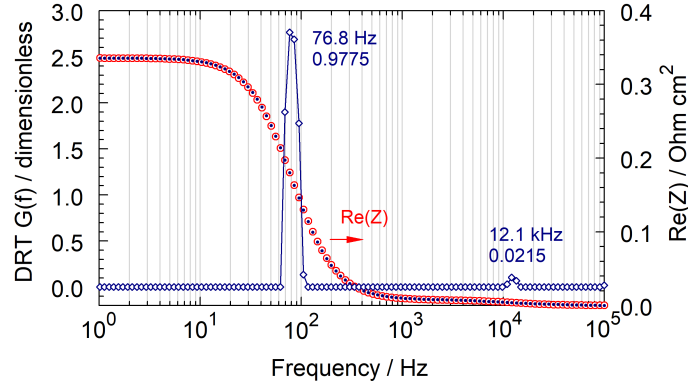


FIG. 5. DRT spectrum  $G(f)$  (open diamonds), where  $G$  is a numerical solution<sup>23</sup> to the DRT equation  $\text{Re}(Z_{ccl}) = R_{ccl} \int_{-\infty}^{\infty} \frac{G(\tau) d \ln \tau}{1 + \omega^2 \tau^2}$  with the impedance Eq.(29). Solid points – real part of impedance, Eq.(29) used for DRT calculation. Open circles –  $\text{Re}(Z_{ccl})$  reconstructed from the DRT. The impedance spectrum  $Z_{ccl}(\omega)$  is calculated with the resolution of 44 points per decade. Numbers at the peaks represent the peak frequency position and the relative peak contribution to the total polarization resistance  $R_{ccl}$ .

### C. Catalyst layer and Nafion film resistivities

Any analytical impedance model in the limit of zero frequency of AC signal leads to the expression for differential resistivity of the system. Calculation of  $\lim_{\tilde{\omega} \rightarrow 0} \tilde{Z}_{ccl}$  with Eq.(29) yields the static CCL resistivity:

$$\tilde{R}_{ccl} = \frac{1}{\sqrt{\xi} \tanh \sqrt{\xi}}, \quad \xi = \tilde{j}_0 \left( 1 - \frac{\tilde{j}_0 \tilde{R}_p \ln \left( \tilde{R}_m / \tilde{R}_p \right)}{2 \tilde{D}_N K_H \tilde{c}_1} \right) \quad (40)$$

Taking into account that the film thickness  $l_N$  is much less than the pore radius, we may write  $\ln(R_m/R_p) = \ln((R_p + l_N)/R_p) = \ln(1 + l_N/R_p) \simeq l_N/R_p$ . With this, Eq.(40) in the dimension form reads

$$R_{ccl} = \frac{l_t}{\sigma_N \sqrt{\xi} \tanh \sqrt{\xi}}, \quad \xi = \frac{j_0 l_t}{\sigma_N b} \left( 1 - \frac{j_0}{j_N^{\text{lim}}} \right) \quad (41)$$

where

$$j_N^{\text{lim}} = \frac{8 F D_N K_H c_1 l_t}{R_p l_N} \quad (42)$$

is the limiting current density due to Nafion film<sup>16</sup>. Note that  $j_N^{\text{lim}}$  is proportional to the CCL thickness  $l_t$ , which is, in turn, proportional to the Pt loading in the electrode. Special cases when the Pt loading is varied keeping the CCL thickness constant<sup>3</sup> are not considered in this work.

For the sake of comparison, it is advisable to expand  $\tilde{R}_{ccl}$ , Eq.(40), over small  $\tilde{j}_0$ . This gives the low-current CCL resistivity, which in the dimension form is

$$R_{ccl}^0 \simeq \frac{l_t}{3 \sigma_N} + \frac{b}{j_0} + \frac{b}{j_N^{\text{lim}}}, \quad j_0 \ll \frac{\sigma_N b}{l_t} \quad (43)$$

The first term on the right side is the proton transport resistivity, the second term is the faradaic resistivity of the ORR, and the last term is the low-current resistivity of the Nafion film:

$$R_N^0 = \frac{b}{j_N^{\text{lim}}} = \frac{b R_p l_N}{8 F D_N K_H c_1 l_t} \quad (44)$$

Figure 6 shows the low-current, Eq.(43), and the general, Eq.(41), dependencies of the cell resistivity on current density. In the region of low currents, the faradaic term (second term in Eq.(43)) dominates. However, in the region of high

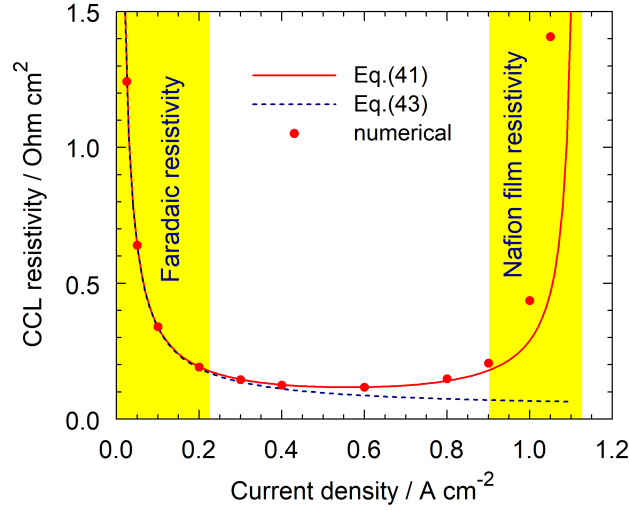


FIG. 6. The general CCL resistivity, Eq.(41), (solid line) and its low-current limit, Eq.(43), (dashed line) vs. current density. Points indicate the values calculated using the numerical model<sup>15</sup> with the pore oxygen diffusivity, GDL oxygen diffusivity and the oxygen stoichiometry set to infinity. Parameters for the calculations are listed in Table I.

Tafel slope $b$ , V	0.03
Nafion film proton conductivity $\sigma_N$ , $\Omega^{-1} \text{ cm}^{-1}$	0.01
Double layer capacitance $C_{dl}$ , F $\text{cm}^{-3}$	20
Oxygen diffusion coefficient in the Nafion film <sup>15</sup> , $D_N$ , $\text{cm}^2 \text{ s}^{-1}$	$10^{-6}$
Dimensionless Henry's constant for $\text{O}_2$ solubility in water at $80^\circ\text{C}$ , $K_H$	$6.76 \cdot 10^{-3}$
Catalyst layer thickness $l_t$ , cm	$3 \cdot 10^{-4}$ (3 $\mu\text{m}$ )
Nafion film thickness <sup>15</sup> $l_N$ , cm	$10 \cdot 10^{-7}$ (10 nm)
Pore radius $R_p$	$100 \cdot 10^{-7}$ (100 nm)
Cell current density $j_0$ , A $\text{cm}^{-2}$	0.1
Pressure	Standard
Cell temperature $T$ , K	$273 + 80$

TABLE I. The cell parameters used in the calculations. Nafion film oxygen diffusivity and thickness correspond to the currents between 100 and 200  $\text{mA cm}^{-2}$  in measurements of<sup>15</sup>.

currents, the resistivity of Nafion film greatly dominates over the other contributions (Figure 6). This effect illustrates the “overlinear” transport loss reported in experiments with low-Pt cells.

Note that Eq.(41) was obtained assuming that  $\tilde{\eta}^0$  is nearly constant along  $\tilde{x}$ . This condition holds if the cell current is small,  $\tilde{j}_0 \ll 1$ , and hence Eq.(41) is valid in the range of cell currents much less than  $\sigma_N b / l_t = 1 \text{ A cm}^{-2}$  (Table I). Nonetheless, at currents  $\tilde{j}_0 \gtrsim 1$ , Eq.(41) qualitatively correctly reproduces the shape of the numerical curve resulting from the complete model<sup>15</sup>, while Eq.(43) is invalid in this range (Figure 6). Small variation of parameters in Eq.(41) makes it possible to achieve perfect fit of the numerical curve.

Close to the limiting current, the behavior of  $R_{ccl}$  is determined solely by the resistivity  $R_N^{\text{lim}}$  of Nafion film:

$$R_{ccl}^{\text{lim}} \simeq R_N^{\text{lim}} \simeq \frac{b}{j_N^{\text{lim}} - j_0}, \quad j_0 \rightarrow j_N^{\text{lim}} \quad (45)$$

Eq.(45) is the leading term in the series expansion of Eq.(41) for  $j_0 \rightarrow j_N^{\text{lim}}$ . From (45) it follows, that the film resistivity

tends to infinity as the working cell current approaches  $j_N^{\text{lim}}$ . Let

$$j_0 = k_j j_N^{\text{lim}}, \quad (1 - \epsilon) \leq k_j < 1, \quad \epsilon \ll 1$$

Taking into account Eq.(42), from (45) we get the following dependence of  $R_N^{\text{lim}}$  on the CCL thickness  $l_t$

$$R_N^{\text{lim}} = \left( \frac{b R_p l_N}{8 F D_N K_H c_1 (1 - k_j)} \right) \frac{1}{l_t} \quad (46)$$

It is interesting to compare Eq.(46) with the recent experimental curve of  $\mathcal{R}_N(L_{Pt})$ , where  $L_{Pt}$  is the Pt loading ( $\text{mg}_{Pt} \text{ cm}^{-2}$ ). To do this, we note that Pt loading of  $0.4 \text{ mg}_{Pt} \text{ cm}^{-2}$  typically corresponds to the CCL thickness of  $l_t^0 = 12 \text{ } \mu\text{m}$ . With this mapping, Eq.(46) can be written as

$$R_N^{\text{lim}} = \left( \frac{b R_p l_N}{8 F D_N K_H c_1 (1 - k_j) l_t^0} \right) \frac{0.4}{L_{Pt}} \quad (47)$$

where  $L_{Pt}$  is in  $\text{mg}_{Pt} \text{ cm}^{-2}$  and  $l_t^0 = 12 \cdot 10^{-4} \text{ cm}$ .

In experiments<sup>14</sup>, a fundamental oxygen transport resistivity  $\mathcal{R}_N$  ( $\text{s cm}^{-1}$ ) of the low-Pt CCL has been measured.  $\mathcal{R}_N$  depends on the CCL thickness and Nafion film parameters only and hence it can be defined as

$$\mathcal{R}_N = \frac{4 F c_1}{b} (1 - k_j) R_N^{\text{lim}} = \left( \frac{R_p l_N}{2 D_N K_H l_t^0} \right) \frac{0.4}{L_{Pt}} \quad (48)$$

Note that Eq.(48) can be derived directly from the low-current Eq.(44).

Eq.(48) multiplied by the fitting parameter  $\alpha$  has been fitted to the experimental points for hydrogen and deuterium from Figure 8a of the paper by Schuler et al.<sup>14</sup> (Figure 7). The product  $D_N K_H = 4.04 \cdot 10^{-8} \text{ cm}^2 \text{ s}^{-1}$  for hydrogen in Nafion 117 membrane has been estimated from experiments of Schalenbach et al.<sup>24</sup> (Figures 4 and 5 in Ref.<sup>24</sup>). The same  $D_N K_H$  has been taken for  $D_2$ . The other two parameters  $R_m$  and  $l_N$  in Eq.(48) are typical for Pt/C electrodes (Table I). Fitting returns the curves in Figure 7 with  $\alpha = 0.648$  for hydrogen and  $\alpha = 0.850$  for  $D_2$ . Both values of  $\alpha$  are close to unity meaning that the combination of parameters in Eq.(48) is close to the real experimental value. Note that the ratio of  $\alpha$ -coefficients for  $D_2$  and  $H_2$  is 1.31, which is close to predicted in<sup>14</sup> value of  $\sqrt{M_{D_2}/M_{H_2}} = \sqrt{2}$ , where  $M_{D_2}, M_{H_2}$  are the atomic masses. Schuler et al.<sup>14</sup> provided arguments in favor of replacing oxygen by hydrogen in the limiting current experiments. According to their work, "... $H_2$  pump presents an oxide-free surface, eliminates water production, and minimizes heat production, thus reducing local environment fluctuations". Thus, comparison with the results of Schuler et al. seems to be the best way for model validation.

It is worth noting that measuring of oxygen diffusivity in Nafion films of the thickness on the order of 10 nm using electrochemical methods is extremely difficult task and literature data on this parameter are scarce<sup>25,26</sup>. It is the goal of this study to simplify measuring of  $D_N$  in operating PEM fuel cell cathodes by means of impedance spectroscopy.

#### D. Equations for Nafion film transport resistivity

It is advisable to compare the equations for Nafion film transport resistivity used in literature. The model above leads to  $\mathcal{R}_N$ , Eq.(48):

$$\mathcal{R}_N = \frac{R_p l_N}{2 D_N K_H l_t}, \quad \text{s cm}^{-1} \quad (49)$$

Nonoyama et al.<sup>9</sup> used the equation for  $\mathcal{R}_N$ , which in our notations reads

$$\mathcal{R}_N = \frac{l_N}{A_{eff} D_N K_H} \quad (50)$$

where  $A_{eff}$  is the effective surface area of Nafion film per unit electrode surface ( $\text{cm}^2/\text{cm}^2$ ). The authors<sup>9</sup> note that  $A_{eff}$  is poorly known and for the estimate they take a value  $A_{eff} = 125$ . Comparing (50) with (49) we see that the model above gives

$$A_{eff} = \frac{2 l_t}{R_p}. \quad (51)$$

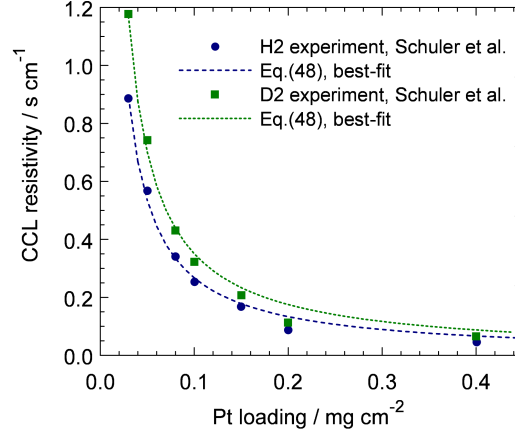


FIG. 7. Eq.(48) fitted to the experimental points for H<sub>2</sub> and D<sub>2</sub> from Figure 8a of Schuler et al.<sup>14</sup>. The product  $D_N K_H$  for hydrogen has been taken from<sup>24</sup>, the other two parameters  $R_p$  and  $l_N$  are taken from Table I. The curve for D<sub>2</sub> is fitted using the same  $D_N K_H$ . The fitting factors for the right side of Eq.(48) are  $\alpha = 0.647$  for H<sub>2</sub> and  $\alpha = 0.850$  for D<sub>2</sub>, their ratio is 1.31, which is close to predicted in<sup>14</sup> value of  $\sqrt{M_{D2}/M_{H2}} = \sqrt{2}$ . Indeed, D<sub>2</sub> diffusivity in Nafion film is  $\sqrt{2}$  times less, than the diffusivity of H<sub>2</sub>, hence the film resistivity to D<sub>2</sub> transport is expected to be  $\sqrt{2}$  times larger. Since for both the curves the product  $D_N K_H$  is the same, the ratio of fitting coefficients should be  $\sqrt{2}$ .

For the standard 12- $\mu\text{m}$  electrode and  $R_p = 100$  nm, the right side of Eq.(51) equals 240, which by the order of magnitude agrees with the value used in<sup>9</sup>. However, for low-Pt electrode,  $A_{eff}$  decreases proportional to  $l_t$ .

Kudo et al.<sup>6</sup> used the following equation

$$\mathcal{R}_N = \frac{l_N}{D_N K_H} + \mathcal{R}_{int} \quad (52)$$

where  $\mathcal{R}_{int}$  takes into account interfacial resistance at the ionomer/Pt and gas/ionomer interface. Comparing Eqs.(52) and (49) we see, that the factor  $R_p/(2l_t)$  is missing in Eq.(52).

Mashio et al.<sup>12</sup> derived the resistivity of Nafion film covering a single carbon particle of the radius  $R_C$ :

$$\mathcal{R}_N = \frac{R_C}{3(1 - \varepsilon_{sp})(1 - \theta)D_N K_H l_t} \left( \frac{1}{r_p} + \frac{1}{l_N} \right)^{-1} \quad (53)$$

where  $\varepsilon_{sp}$  is the volume fraction of the secondary pores in the carbon particle,  $\theta$  is the fraction of carbon particle surface covered by Nafion film. This expression is derived for HiSpec type of carbon support containing nano-channels in which Pt particles are buried. Eq.(53) cannot be directly compared to Eq.(49) obtained for carbon support of Vulcan type, with Pt particles on the outside surface of carbon support. Nonetheless, Eq.(53) shows the same scaling as Eq.(49): in the limit of  $l_N \ll r_p$ , from Eq.(53) we get  $\mathcal{R}_N \sim l_N/(D_N K_H l_t)$ .

Schuler et al.<sup>14</sup> used the following expression for the for the Nafion film resistance

$$\mathcal{R}_N = \frac{\mathcal{R}_{Local}}{\theta a_v l_t} \quad (54)$$

where  $\mathcal{R}_{local}$  is the local mass transport resistance close to the Pt particle,  $\theta$  is the focusing factor which takes into account geometry of agglomerate, and  $a_v$  is the Pt area on agglomerate external surface area per unit CL volume. The parameter  $\mathcal{R}_{Local}/(\theta a_v)$  was obtained as a slope of the dependence of the total CCL resistance vs inverse fraction of ECSA in the electrode. In our recent paper<sup>15</sup>,  $\mathcal{R}_N$  was estimated simply as  $l_N/D_N$ . From (49) it follows that these values should be multiplied by  $R_p/(2K_H l_t)$ . With the data from Table I, this factor is 2.47.

Finally we note that the equations for Nafion film resistance contain the oxygen permeation coefficient  $D_N K_H$ . Generally,  $D_N$  and  $K_H$  could be considered as time-dependent parameters governed by oxygen adsorption/solubility, water sorption/desorption and related structural changes of ionomer<sup>25,27,28</sup>. Incorporation of these processes would be interesting model extension.

#### IV. CONCLUSIONS

A recent single-pore model for impedance of the cathode catalyst layer (CCL) in a low-Pt PEM fuel cell is analyzed. The CCL is modeled by a single cylindrical pore surrounded by thin Nafion film separating the open pore volume from the coaxial Pt cylinder. Assuming fast oxygen transport along the pore and nearly flat shape of the ORR overpotential, the model is solved analytically. The obtained expression for CCL impedance takes into account faradaic process at the film/Pt interface and the impedance due to proton and oxygen transport in the Nafion film. Further, the low-current expression for film transport impedance is derived. The characteristic frequency of oxygen transport in the film is independent on film oxygen transport parameters and it is only 1.73 times less than the frequency of charge-transfer impedance. This impedes separation of the film-transport and faradaic processes by EIS at low currents.

In the limit of zero frequency the expression for the CCL resistivity  $R_{ccl}$  is derived.  $R_{ccl}$  rapidly growth to infinity as the cell current approaches limiting current density in the Nafion film. For a typical set of parameters, this current density is about  $1 \text{ A cm}^{-2}$ . The model dependence of the film transport resistance  $R_N$  on Pt loading (CCL thickness) fits well the recent experimental data from Schuler et al.<sup>14</sup>.

#### Appendix A: Numerical method for DRT calculation

The method discussed below solves the real or imaginary part of the general DRT equation

$$Z = R_{HFR} + R_{pol} \int_{-\infty}^{\infty} \frac{G(\tau) d \ln \tau}{1 + i\omega\tau} \quad (\text{A1})$$

for the dimensionless DRT spectrum  $G(\tau)$ . Consider for definiteness the real part of Eq.(A1)

$$Z_{re} - R_{HFR} = R_{pol} \int_{-\infty}^{\infty} \frac{G(\tau) d \ln \tau}{1 + \omega^2 \tau^2} \quad (\text{A2})$$

We approximate integral in Eq.(A2) on a log-scale grid, which gives a linear system of equations of the form

$$\mathbf{A} \vec{G} = \vec{b}, \quad \vec{b} \equiv \vec{Z}_{re} - R_{HFR} \quad (\text{A3})$$

where the components of matrix  $\mathbf{A}$  are given by

$$A_{m,n} = \frac{R_{pol} \delta \ln(\tau_n)}{1 + \omega_m^2 \tau_n^2}, \quad \delta \ln(\tau_n) = \ln(\tau_{n+1}) - \ln(\tau_n), \quad \tau_n = 1/\omega_n \quad (\text{A4})$$

and  $G_n, n = 1, \dots, N$  is a vector to be solved for. Further, we cast Eq.(A3) into the Tikhonov regularization form

$$(\mathbf{A}^T \mathbf{A} + \lambda_T \mathbf{I}) \vec{G} - \mathbf{A}^T \vec{b} = 0 \quad (\text{A5})$$

where  $\mathbf{A}^T$  is the transposed  $\mathbf{A}$ ,  $\mathbf{I}$  is the identity matrix, and  $\lambda_T$  is the regularization parameter. Eq.(A5) is solved using a non-negative least-squares method<sup>29</sup> which seeks for the vector  $\vec{G}$  satisfying to

$$\arg \min_G \left\{ (\mathbf{A}^T \mathbf{A} + \lambda_T \mathbf{I}) \vec{G} - \mathbf{A}^T \vec{b} \right\}, \quad \vec{G} \geq 0 \quad (\text{A6})$$

where  $\vec{G} \geq 0$  means that all components of vector  $\vec{G}$  must be non-negative. Eq.(A6) is solved using the *nnls* procedure from the SciPy library. The Python code and implementation details can be found at<sup>23</sup> (see the file "DRT\_Gfun\_nnls\_\*.zip").

- <sup>1</sup>Y. Ono, T. Mashio, S. Takaichi, A. Ohma, H. Kanesaka and K. Shinohara, *The Analysis of Performance Loss with Low Platinum Loaded Cathode Catalyst Layers*, ECS Transactions **28** (2010), pp. 69–78
- <sup>2</sup>T. A. Greszler, D. Caulk and P. Sinha, *The Impact of Platinum Loading on Oxygen Transport Resistance*, J. Electrochem. Soc. **159** (2012), pp. F831–F840
- <sup>3</sup>J. P. Owejan, J. E. Owejan and W. Gu, *Impact of Platinum Loading and Catalyst Layer Structure on PEMFC Performance*, J. Electrochem. Soc. **160** (2013), pp. F824–F833
- <sup>4</sup>A. Z. Weber and A. Kusoglu, *Unexplained Transport Resistances for Low-Loaded Fuel-Cell Catalyst Layers*, J. Mater. Chem. A **2** (2014), pp. 17207–17211
- <sup>5</sup>A. Kongkanand and M. F. Mathias, *The Priority and Challenge of High-Power Performance of Low-Platinum Proton-Exchange Membrane Fuel Cells*, Phys. Chem. Lett. **7** (2016), pp. 1127–1137
- <sup>6</sup>K. Kudo, R. Jinnouchi and Y. Morimoto, *Humidity and Temperature Dependences of Oxygen Transport Resistance of Nafion Thin Film on Platinum Electrode*, Electrochimica Acta **209** (2016), pp. 682–690
- <sup>7</sup>A. T. S. Freiberg, M. C. Tucker and A. Z. Weber, *Polarization Loss Correction Derived from Hydrogen Local-Resistance Measurement in Low Pt-Loaded Polymer-Electrolyte Fuel Cells*, Electrochem. Comm. **79** (2017), pp. 14–17
- <sup>8</sup>T. Muzaffar, T. Kadyk and M. Eikerling, *Tipping Water Balance and the Pt Loading Effect in Polymer Electrolyte Fuel Cells: A Model-based Analysis*, Sustainable Energy & Fuels **2** (2018), pp. 1189–1196
- <sup>9</sup>N. Nonoyama, S. Okazaki, A. Z. Weber, Y. Ikogi and T. Yoshida, *Analysis of Oxygen-Transport Diffusion Resistance in Proton-Exchange-Membrane Fuel Cells*, J. Electrochem. Soc. **158** (2011), pp. B416–B423
- <sup>10</sup>L. Chen, R. Zhang, P. He, Q. Kang, Y.-L. He and W.-Q. Tao, *Nanoscale Simulation of Local Gas Transport in Catalyst Layers of Proton Exchange Membrane Fuel Cells*, J. Power Sources **400** (2015), pp. 114–125
- <sup>11</sup>M. Moore, P. Wardlaw, P. Dobson, J. J. Boisvert, A. Putz, R. J. Spiteri and M. Secanell, *Understanding the Effect of Kinetic and Mass Transport Processes in Cathode Agglomerates*, J. Electrochem. Soc. **161** (2014), pp. E3125–E3137
- <sup>12</sup>T. Mashio, H. Idena, A. Ohma and T. Tokumasu, *Modeling of Local Gas Transport in Catalyst Layers of PEM Fuel Cells*, J. Electroanal. Chem. **790** (2017), pp. 27–39
- <sup>13</sup>L. Hao, K. Moriyama, W. Gu and C.-Y. Wang, *Modeling and Experimental Validation of Pt Loading and Electrode Composition Effects in PEM Fuel Cells*, J. Electrochem. Soc. **162** (2015), pp. F854–F867
- <sup>14</sup>T. Schuler, A. Chowdhury, A. T. Freiberg, B. Sneed, F. B. Spangler, M. C. Tucker, K. L. More, C. J. Radke and A. Z. Weber, *Fuel-Cell Catalyst-Layer Resistance via Hydrogen Limiting-Current Measurements*, J. Electrochem. Soc. **166** (2019), pp. F3020–F3031
- <sup>15</sup>T. Reshetenko and A. Kulikovskiy, *A Single-Pore Model for Cathode Catalyst Layer Impedance: The Effect of Nafion Film on PEM Fuel Cell Performance*, RSC Adv. **9** (2019), pp. 38797–38806
- <sup>16</sup>A. Kulikovskiy, *The Effect of Nafion Film on the Cathode Catalyst Layer Performance in a Low-Pt PEM Fuel Cell*, Electrochem. Comm. **103** (2019), pp. 61–65
- <sup>17</sup>A. Kulikovskiy and T. Reshetenko, *Correction: A Single-Pore Model for Cathode Catalyst Layer Impedance: The Effect of Nafion Film on PEM Fuel Cell Performance*, RSC Adv., 2019, 9, 38797, doi:10.1039/C9RA07794D, RSC Adv. **11** (2021), pp. 6764 – 6765
- <sup>18</sup>A. A. Kulikovskiy, *One-Dimensional Impedance of the Cathode Side of a PEM Fuel Cell: Exact Analytical Solution*, J. Electrochem. Soc. **162** (2015), pp. F217–F222
- <sup>19</sup>A. A. Kulikovskiy and M. Eikerling, *Analytical Solutions for Impedance of the Cathode Catalyst Layer in PEM Fuel Cell: Layer Parameters from Impedance Spectrum Without Fitting*, J. Electroanal. Chem. **691** (2013), pp. 13–17
- <sup>20</sup>A. Kulikovskiy and O. Shamardina, *A Model for PEM Fuel Cell Impedance: Oxygen Flow in the Channel Triggers Spatial and Frequency Oscillations of the Local Impedance*, J. Electrochem. Soc. **162** (2015), pp. F1068–F1077
- <sup>21</sup>A. A. Kulikovskiy, *A Simple Physics-Based Equation for Low-Current Impedance of a PEM Fuel Cell Cathode*, Electrochim. Acta **196** (2016), pp. 231–235
- <sup>22</sup>T. Reshetenko and A. Kulikovskiy, *Distribution of Relaxation Times: A Tool for Measuring Oxygen Transport Resistivity of a Low-Pt PEM Fuel Cell Cathode*, J. Electrochem. Soc. **167** (2020), p. 144505
- <sup>23</sup>*DRT Python codes* (2020),  
URL: <https://github.com/akulikovsky/DRT-Python-code>
- <sup>24</sup>M. Schalenbach, T. Hoefner, P. Paciok, M. Carmo, W. Lueke and D. Stolten, *Gas Permeation through Nafion. Part 1: Measurements*, J. Phys. Chem. C **119** (2015), pp. 25145–25155
- <sup>25</sup>D. Novitski and S. Holdcroft, *Determination of O<sub>2</sub> Mass Transport at the Pt / PFSA Ionomer Interface under Reduced Relative Humidity*, ACS Appl. Mater. Interfaces **7** (2015), pp. 27314–27323
- <sup>26</sup>A. Kusoglu and A. Z. Weber, *New Insights into Perfluorinated Sulfonic-Acid Ionomers*, Chem. Rev. **117** (2017), pp. 987–1104
- <sup>27</sup>A. Kusoglu, M. A. Modestino, A. Hexemer, R. A. Segalman and A. Z. Weber, *Subsecond Morphological Changes in Nafion during Water Uptake Detected by Small-Angle X-ray Scattering*, ACS Macro Lett. **1** (2012), pp. 33–36
- <sup>28</sup>K.-D. Kreuer, *The Role of Internal Pressure for the Hydration and Transport Properties of Ionomers and Polyelectrolytes*, Solid State Ionics **252** (2013), pp. 93–101
- <sup>29</sup>C. L. Lawson and R. J. Hanson, *Solving Least Squares Problems* (SIAM, Philadelphia, 1995)

## Nomenclature

$\sim$	Marks dimensionless variables
$b$	ORR Tafel slope, V
$C_{dl}$	Double layer volumetric capacitance, F cm <sup>-3</sup>
$c$	Oxygen molar concentration in the pore, mol cm <sup>-3</sup>
$c_N$	Oxygen molar concentration in the Nafion film, mol cm <sup>-3</sup>
$c_h^{in}$	Reference (inlet) oxygen concentration, mol cm <sup>-3</sup>
$D_p$	Oxygen diffusion coefficient in the pore, cm <sup>2</sup> s <sup>-1</sup>
$D_N$	Oxygen diffusion coefficient in the Nafion film, cm <sup>2</sup> s <sup>-1</sup>
$E$	Auxiliary parameter, Eq.(27)
$F$	Faraday constant, C mol <sup>-1</sup>
$i_*$	ORR volumetric exchange current density, A cm <sup>-3</sup>
$i$	Imaginary unit
$j$	Local proton current density along the pore, A cm <sup>-2</sup>
$j_N^{lim}$	Limiting current density due to oxygen transport in Nafion film, A cm <sup>-2</sup>
$j_*$	Characteristic current density of proton transport, A cm <sup>-2</sup> , Eq.(8)
$j_0$	Cell current density, A cm <sup>-2</sup>
$K_H$	Dimensionless Henry's constant for oxygen solubility in water, mol/mol
$k_j$	$= j_0/j_N^{lim}$ , ratio of the cell current density to the limiting current density
$L_{Pt}$	Pt loading, mg <sub>Pt</sub> cm <sup>-2</sup>
$l_t$	Pore length (CCL thickness), cm
$l_N$	Nafion film thickness, cm
$N_N$	Radial oxygen flux in the Nafion film, mol cm <sup>-2</sup> s <sup>-1</sup>
$q$	Auxiliary parameter, Eq.(27)
$\mathcal{R}_N$	Transport resistivity of Nafion film, s cm <sup>-1</sup>
$R_{ccl}$	Catalyst layer resistivity, Ohm cm <sup>2</sup>
$R_m$	Radius of a Pt/C tube, cm
$R_N$	Nafion film transport resistivity, Ohm cm <sup>2</sup>
$R_p$	Pore radius, cm
$r$	Radial coordinate, cm
$t_*$	Characteristic time, s, Eq.(8)
$x$	Coordinate along the pore, cm
$Z$	Impedance, Ohm cm <sup>2</sup>
$Z_{ccl}$	CCL impedance, Ohm cm <sup>2</sup>
$Z_N$	Nafion film impedance, Ohm cm <sup>2</sup>

### Subscripts:

0	Membrane/CCL interface
1	CCL/GDL interface
<i>ccl</i>	Cathode catalyst layer
<i>m</i>	Pt/C (metal) surface
<i>N</i>	Nafion film
<i>p</i>	Pore/Nafion film interface

### Superscripts:

- 0 Steady-state value  
 1 Small-amplitude perturbation  
 $\infty$  Some parameter tends to  $\infty$   
 lim Limiting

**Greek:**

- $\gamma_p = 2/\tilde{R}_p$   
 $\gamma_m = 2\tilde{R}_m/\tilde{R}_p^2$   
 $\varepsilon_*$  Dimensionless Newman's reaction penetration depth, Eq.(12)  
 $\eta$  ORR overpotential, positive by convention, V  
 $\mu$  Dimensionless parameter, Eq.(12)  
 $\xi$  Dimensionless parameter, Eq.(40)  
 $L_{Pt}$  Pt loading, mg cm<sup>-2</sup>  
 $\psi$  Dimensionless parameter. Eq.(30)  
 $\sigma_N$  Nafion film proton conductivity, S cm<sup>-1</sup>  
 $\omega$  Angular frequency of the AC signal, s<sup>-1</sup>